*Aceh Int. J. Sci. Technol.*, 10(2) 100-116
August, 2021
doi: 10.13170/aijst.10.2.18096

Aceh International Journal of Science and Technology
ISSN: p-2088-9860; e-2503-2398
Journal homepage: http://jurnal.unsyiah.ac.id/aijst

# Use of Reactivated Spent FCC Catalyst as Adsorbent for Lead (II) Ions from Refinery-based Simulated Wastewater

**Abdulkareem Abubakar[1]*, Ijai Ezekiel Waba[1], Suleiman Yunusa[1], Zaharaddeen Sani Gano[2]**
[1]Department of Chemical Engineering, Ahmadu Bello University, Zaria, Nigeria.
[2]Petrochemical and Allied Department, National Research Institute for Chemical Technology, Zaria, Nigeria
*Corresponding author: abubakara@abu.edu.ng

Received : September 24, 2020
Accepted: September 09, 2021
Online : September 09, 2021

**Abstract –** Improper handling of wastewater from various industries causes environmental pollution. Hence, this study involved using a reactivated spent FCC catalyst, a cheap and reliable adsorbent for $Pb^{2+}$ removal from refinery-based simulated wastewater. In contrast, response surface methodology (RSM) was used to determine the optimum operating condition. The adsorptive capacity of the reactivated spent FCC catalyst was observed using different parameters such as temperature, pH, adsorbent dosage, and contact time. At the end of the study, it was found that the optimum condition for removing $Pb^{2+}$ was at pH of 7, adsorbent dose of 1.75 g, contact time of 75 mins, and temperature of 117 $^{o}$C. At this condition, the maximum removal efficiency of $Pb^{2+}$ was found to be 100 %. A quadratic model equation via central composite design under the RSM was developed to predict the $Pb^{2+}$ removal from all the input parameters. Based on the F-statistic values, the temperature had the greatest influence on the removal of $Pb^{2+}$ while adsorbent dosage and contact time were also significant.

**Keywords:** Heavy metal removal; spent FCC catalyst; adsorption; optimization; response surface methodology

## Introduction

Rapid industrialization has led to various wastes such as dyes, surfactants, and certain metals from various industrial processes. Unlike organic pollutants, heavy metals such as chromium, nickel, lead, etc., are non-biodegradable in the environment. This leads to disturbance of the ecosystem and possible accumulation in the human body causing numerous problems. These heavy metals are found as by-products of several industries: paint, electroplating, metal finishing, fertilizer, electrical, refineries, pigment industries, wood manufacturing, etc. (Manzoor *et al.*, 2013).

Among the numerous toxic heavy metals, lead is known to be a common and highly toxic pollutant. It is found especially in battery manufacturing, metal plating, and oil refining industries (Yurtsever and Sengil, 2008). It accumulates in the human body through ingestion, inhalation, or skin absorption, concentrating in the brain, bones, kidneys, and muscles, and causing serious disorders such as anemia, nervous disorder, kidney disease, and death (Kazi *et al.*, 2008; Afridi *et al.*, 2006). Although it can be used in place of calcium as an essential mineral for teeth and bones, a high concentration of lead damages cognitive development in children (Yarkandi, 2014).

A number of wastewater treatment techniques have been employed to remove heavy metal ions (Fu and Wang, 2013). These include chemical precipitation (Wang *et al.*, 2018), ion exchange (Kang *et al.*, 2004; Zamora-Ledezma *et al.*, 2021), membrane filtration and electrochemical treatment (Zhou *et al.*,

2015; Qasem *et al.*, 2021), and adsorption (Castro *et al.*, 2018), which is considered as a low-cost, high-efficient, eco-friendly and easy to operate technique (Yen *et al.*, 2017). In searching for a simple, eco-friendly, and effective adsorbent for the removal of heavy metals from wastewater, the use of several adsorbents has also been studied. These studies include the use of Annona reticulata Linn peel microparticles (Saranya *et al.,* 2017), chitosan composite (Begum *et al.,* 2021), Biochar (Qiu *et al.,* 2021), $Fe_3O_4$-$FeMoS_4$ based LDH adsorbent (Behbahani *et al.,* 2021), subglebal tissue of the mosaic puffball (*Handkea utriformis*) (Milošević *et al.,* 2021), and polypyrrole wrapped oxidized MWCNTs nanocomposites (Bhaumik *et al.*, 2016). Also, spent lithium-ion batteries (Zhang *et al.,* 2021b), maple sawdust (Yu *et al.*, 2003), Avocado seed hydrochar (Dhaouadi *et al.,* 2021), date stones activated carbon (Kaoah *et al.*, 2015), sulfonated polynorbornene dicarboximides (Ruiz *et al.,* 2021). Colocasia esculenta leaves powder (Nakkeeran *et al.*, 2016) has been used. Others include chemically modified Swietenia mahagoni (Rangabhashiyam *et al.*, 2016), fruit peel of Trewia nudiflora (Bhattacharya *et al.,* 2013), cigarette butts (Zhang *et al.,* 2021a), acid-modified granular activated carbon (Daoud *et al.,* 2015), β-$Ca_2P_2O_7$ (Griesiute *et al.,* 2021), acorn peel (Kuppusamy *et al.,* 2016), polyaniline (PANI)-based adsorbents (Samadi *et al.,* 2021), chitosan–lignin composites (Nair *et al.,* 2014), etc.

Various research works specifically on removing lead (II) ions from wastewater using various adsorbents have also been published. Some of them are presented in Table 1.

Table 1. Some past works on $Pb^{2+}$ adsorption from wastewater

| Author and Year | Adsorbent |
|---|---|
| Mengistie *et al.* (2008) | Activated carbon |
| Kam *et al.* (2011) | Synthesized zeolite |
| Xu and Wang (2012) | Hydrolytic lignin |
| Ahmad *et al.* (2014) | Saudi Arabian clay |
| Erdem *et al.* (2014) | Waste biomass |
| Ogunleye *et al.* (2014) | Banana stalk |
| Yarkandi (2014) | American bentonite |
| Dakhil (2015) | Rice husk |
| El-Naggar *et al.* (2018) | Kaolinite/Smectite |
| Ali (2019) | Concrete demolition waste |
| Kuganathan *et al.* (2021) | Pristine and B, Si and N-doped graphene |
| Claros *et al.* (2021) | $MnO_2$ nanowires |
| Gao *et al.* (2021b) | Alginate/melamine/chitosan aerogel |
| Kim *et al.* (2021) | Basic oxygen furnace (BOF) slag |
| Kuganathan *et al.* (2021) | Pristine and B, Si and N-doped graphene |
| Pelalak *et al.*(2021) | Oakwood ash/GO/$Fe_3O_4$ composites |
| Ramos-Guivar *et al.* (2021) | EDTA functionalized γ-$Fe_2O_3$ nanoparticles |
| Shen *et al.* (2021) | Polyethylene, polypropylene, and polymethylmethacrylate |
| Wang *et al.* (2021) | Loess |
| Zhao *et al.* (2021) | Cellulose nanofiber (CNF) |

Recently, spent FCC catalysts are being produced in the refineries in large quantities as solid waste because of the great demand for light and high-quality transportation fuels. Previously, these spent catalysts have been disposed of as landfills in approved dumping sites (Cerqueira *et al.*, 2008). However, due to metals such as Co, Ni, and V on the spent catalysts, they are included in the list of toxic wastes recognized in many countries. Hence, disposal must be carried out in accordance with environmental regulations. Fortunately, the spent FCC catalyst can be used effectively as a very low-cost adsorbent in wastewater treatment. This is because of its microporous nature and the presence of trivalent $Al^{3+}$ at tetrahedral sites, which gives a framework of the catalysts a negative charge. This negative charge has

to be compensated by an extra framework cation, and this is where its ability to adsorb positively charged cation like $Pb^{2+}$ comes into play (Bingre *et al.,* 2018).

Therefore, the work aimed to explore the unique advantage of the spent catalysts to adsorb $Pb^{2+}$ from refinery-based simulated wastewater. In addition, response surface methodology (RSM) via central composite design (CCD) was deployed to determine optimum operating conditions for the $Pb^{2+}$ removal.

## Materials and Methods

### Materials

A spent FCC catalyst sample (E-cat) was obtained from the Kaduna Refining and Petrochemical Company (KRPC), Kaduna, Nigeria, and was treated to remove coke deposits and contaminant metals. The detailed method of the treatment can be found in our earlier published work (Waba *et al.*, 2020). Lead (II) nitrate ($Pb(NO_3)_2$, 97w/w% Purity, JHD) was used to simulate wastewater, 1M $HNO_3$ (98w/v% Purity, CDH) and 1M NaOH (97w/w% purity, CDH) solutions were used to vary the pH of the simulated wastewater during the adsorption study, Design-Expert version 10 was used to design the experiment.

A magnetic stirrer (78HW-1) was used to facilitate contact between adsorbent (i.e., treated or reactivated spent FCC catalyst) and simulated wastewater, and atomic absorption spectrometer (AAS, model number iCE 3000 AA01122804 v1.30) was used to measure the concentration of heavy metals present in wastewater before and after adsorption.

### Preparation of simulated wastewater

Stock $Pb^{2+}$ solution was prepared from $Pb(NO_3)_2$ by dissolving 12.5g of $Pb(NO_3)_2$ in 100ml of deionized water to obtain a 1000mg/L concentration of $Pb^{2+}$. 0.5ml of the stock $Pb^{2+}$ solution was measured and placed in a 1000-mL volumetric flask. The content was then made up to the mark using deionized water to obtain 0.5mg/L of $Pb^{2+}$ solutions, which served as the simulated wastewater. The choice of the simulated wastewater was to approximate the wastewater in Warri Refining and Petrochemical Company (WRPC), Warri, Delta State, Nigeria, which contains 0.47mg/L (Olayebi and Adebayo, 2017).

### Adsorption process

For the adsorption experiment, 50 mL of the simulated wastewater was used in each run. In each experimental run, the adsorbent was mixed with the simulated wastewater in conical flasks and stirred by the magnetic stirrer at 150 rpm. Then the treated wastewater was separated from the adsorbent using a 45-micron Whatman filter paper. After that, AAS was employed to quantify the residual metal ion concentration in the treated wastewater. The following equation was used to compute the amount of $Pb^{2+}$ removal.

$$Pb^{2+}\ \text{Removal} = \left[1 - \frac{C_t}{C_o}\right] \times 100 \quad (1)$$

where $C_o$ and $C_t$ are the initial concentration and concentration at any time of $Pb^{2+}$, mg/L.

### Optimization of operating conditions for $Pb^{2+}$ removal

To optimize the removal of $Pb^{2+}$ from refinery-based simulated wastewater using reactivated spent FCC catalyst, variables such as pH (-), adsorbent dosage (g), time (min.), and temperature ($^oC$) were considered. These variables, also known as factors, were denoted as $X_1, X_3, X_3$ and $X_4$ respectively. Central composite design (CCD) under the RSM was employed to determine the optimum condition and the mutual interaction effects of the factors on the response (i.e., $Pb^{2+}$ removal). The CCD is characterized by three types of points: factorial point (coded as –1, 0, and +1), axial point (coded as

$\pm\alpha$), and center point (denoted as 0). Equations (2a) and (2b) were used to calculate the value of $\alpha$ for 2-level 'full' and 'small' CCD options, respectively.

$$\alpha = \left[2^{k}\right]^{0.25} \tag{2}$$

$$\alpha = [2^{k-1}]^{0.25} \tag{3}$$

where $k$ is the number of factors.

Since second-order polynomial regression model equation is known to be best suited for CCB (Anupam *et al.*, 2011; Ackay and Anagun, 2013; Daoud *et al.*, 2015; Sada, 2018; Ani *et al.*, 2019), the removal efficiency of $Pb^{2+}$ was therefore represented in terms of the independent variables as:

$$Y = \beta_o + \sum_{i=1}^{P} \beta_1 X_1 + \sum_{i=1}^{P} \beta_{11} X_1^2 + \ldots + \sum_{1<j} \beta_{11} X_1 X_j + \epsilon \tag{4}$$

where Y is the predicted response (i.e., $Pb^{2+}$ removal efficiency), $X_i$ and $X_j$ are independent variables, $\epsilon$ is the error, $\beta_o$ is the constant coefficient, $\beta_i$ is the coefficient for linear interaction effect, and $\beta_{ii}$ are coefficients for the quadratic interaction effect.

Meanwhile, the coded (X) and actual factors are related according to the following equation.

$$X = [X_i - X_o]/\Delta X \tag{5}$$

where $X_i$ denotes the actual value of variable $i$, $X_o$ denotes value of $X_i$ at the center point, and $\Delta X$ denotes step change.

Table 2 shows the inputted design ranges for the four factors investigated during the adsorption of $Pb^{2+}$ from the simulated wastewater using reactivated spent FCC catalyst. Based on the fact that the CCD can effectively optimize parameters with a minimum number of experiments (Anupam *et al.*, 2011), the 'small' CCD option was the chosen design criteria. The total number of experimental runs was 21, consisting of eight axial experimental runs, five center experimental runs, and eight factorial experimental runs. The actual ranges of the input factors obtained from the CCD are presented with their corresponding output response (i.e.% $Pb^{2+}$ removal) in the result and discussion section.

Table 2. Design ranges of the operating parameters

| Name | Symbol | Units | Type | Low | High |
|---|---|---|---|---|---|
| pH | $X_1$ | _ | Factor | 4 | 10 |
| Adsorbent | $X_2$ | g | Factor | 1 | 2.5 |
| time | $X_3$ | min. | Factor | 60 | 90 |
| temperature | $X_4$ | $^oC$ | Factor | 50 | 100 |

## Results

### Adsorption study

Figure 1(a and b) presents the micrographs of the reactivated spent FCC catalyst before and after adsorption, respectively. In Figure 1(a), the reactivated spent FCC catalyst's microstructure, presented at 80µm and 1000x magnification, showed some tiny crystallite spikes on the catalyst surface. This image is similar to the one reported in Le *et al.* (2019), where they reactivated the spent FCC catalyst with hydrochloric acid and oxalic acid. According to them, these tiny spikes were responsible for the removal of contaminant metals. Figure 1(b) presents the microstructure of the reactivated spent FCC catalyst at 80µm and 1000x magnification. White patches were observed on the catalyst surface at the

tiny crystallite spikes sites. The appearance of these patches can be attributed to the adsorption of $Pb^{2+}$ on the catalyst's active sites. This image is in agreement with the image reported by Chen *et al.* (2004) when they tested two different samples of spent FCC Ecat and Epcat catalyst for the consumption of calcium hydroxide.

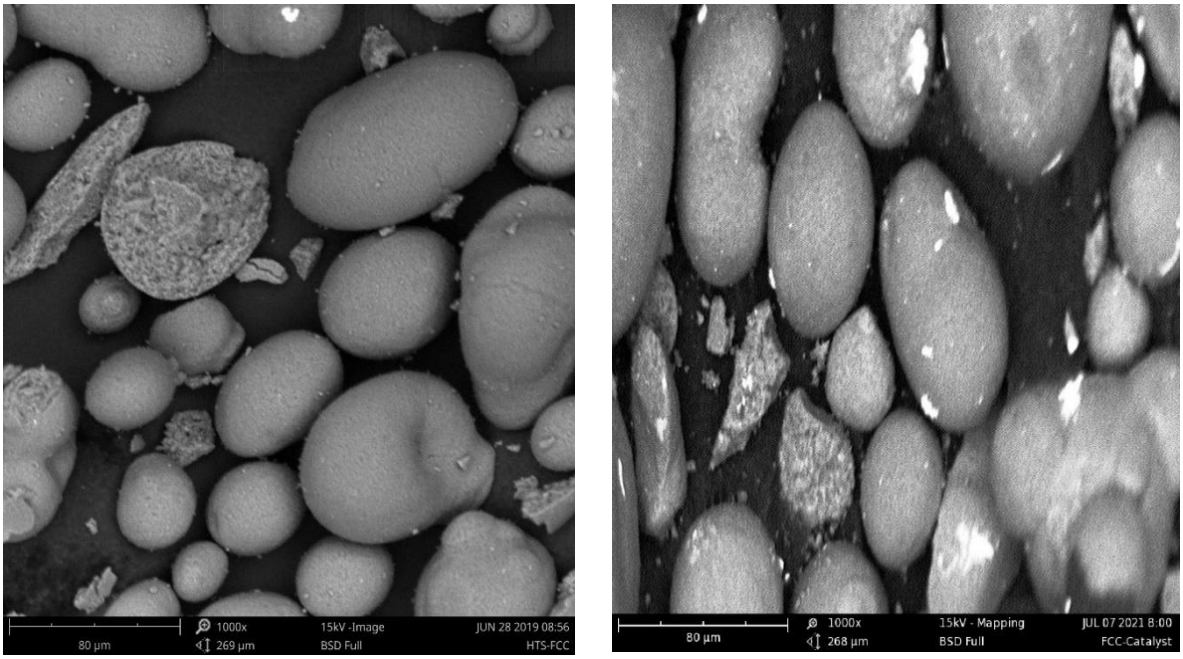


**(a)** **(b)**

Figure 1. SEM micrographs of FCC catalyst (a) reactivated spent FCC catalyst before adsorption, (b) reactivated spent FCC catalyst after adsorption.

Table 3 presents the experimental runs for this work as designed by the CCD. This table observed a progressive increase in $Pb^{2+}$ removal when the adsorbent dose was varied from 0.49g to 3.01g per 50 mL of working solution, with other factors fairly constant. Effect of temperature on the adsorption system reveals that the adsorption of $Pb^{2+}$ on the reactivated spent FCC catalyst was endothermic because of its proportionality with increasing temperature. When the system temperature was increased from 32.96 to 117 $^{o}$C, $Pb^{2+}$ removal increased sharply from 18.4 to 100 %. It was also observed that the $Pb^{2+}$ removal increased from 49.4343 to 100 % when contact time between the simulated wastewater and adsorbent was increased from 49.77 to 100.23 mins, with other factors fairly constant. Variation in the pH from 1.95 to 12.05 when time, temperature, and adsorbent dosage were kept fairly constant showed that the maximum $Pb^{2+}$ removal was at a pH of 7. Therefore, as presented in Figure 2, the maximum $Pb^{2+}$ removal was 100 % observed at run 15, which coincides with the operating condition: pH = 7, adsorbent dose = 1.75 g, contact time = 75 min. and temperature = 117 $^{o}$C. Conversely, the minimum $Pb^{2+}$ removal was recorded at run 18 coinciding with operating condition: pH = 1.95, adsorbent dose = 1.75 g, contact time = 75 min. and temperature = 75 $^{o}$C.

**Model summary statistics**

The statistical results are summarized in Table 4. As expected, the quadratic model showed the best fit and was therefore suggested. In the absence of the quadratic model, the linear model can represent the relationship between the factors and the response through statistical data such as R2 and adjusted R2.

Table 3. CCD matrix with experimental and predicted responses

| Std | Run | $X_1$ (-) | $X_2$ (g) | $X_3$ (min) | $X_4$ (°C) | Coded Values | | | | $Pb^{2+}$ Removal (%) | |
|---|---|---|---|---|---|---|---|---|---|---|---|
| | | | | | | $X_1$ | $X_1$ | $X_1$ | $X_1$ | Exp. | Predicted |
| 6 | 1 | 4 | 1 | 90 | 50 | -1 | -1 | 1 | -1 | 33.33 | 38.36 |
| 11 | 2 | 7 | 0.49 | 75 | 75 | 0 | $-\alpha^*$ | 0 | 0 | 39.89 | 37.36 |
| 17 | 3 | 7 | 1.75 | 75 | 75 | 0 | 0 | 0 | 0 | 58.30 | 58.52 |
| 8 | 4 | 4 | 1 | 60 | 50 | -1 | -1 | -1 | -1 | 23.25 | 21.78 |
| 4 | 5 | 4 | 2.5 | 60 | 100 | -1 | 1 | -1 | 1 | 58.25 | 52.38 |
| 12 | 6 | 7 | 3.01 | 75 | 75 | 0 | $\alpha$ | 0 | 0 | 60.78 | 64.94 |
| 10 | 7 | 12.05 | 1.75 | 75 | 75 | $\alpha$ | 0 | 0 | 0 | 18.27 | 21.34 |
| 1 | 8 | 10 | 2.5 | 90 | 50 | 1 | 1 | 1 | -1 | 56.40 | 57.44 |
| 5 | 9 | 10 | 1 | 60 | 100 | 1 | -1 | -1 | 1 | 39.72 | 38.66 |
| 15 | 10 | 7 | 1.75 | 75 | 32.96 | 0 | 0 | 0 | $-\alpha$ | 18.40 | 17.72 |
| 2 | 11 | 10 | 2.5 | 60 | 50 | 1 | 1 | -1 | -1 | 47.76 | 40.86 |
| 14 | 12 | 7 | 1.75 | 100.2 | 75 | 0 | 0 | $\alpha$ | 0 | 92.76 | 85.85 |
| 21 | 13 | 7 | 1.75 | 75 | 75 | 0 | 0 | 0 | 0 | 58.30 | 58.52 |
| 3 | 14 | 10 | 1 | 90 | 100 | 1 | -1 | 1 | 1 | 54.42 | 55.24 |
| 16 | 15 | 7 | 1.75 | 75 | 117.1 | 0 | 0 | 0 | $\alpha$ | 100 | 99.32 |
| 18 | 16 | 7 | 1.75 | 75 | 75 | 0 | 0 | 0 | 0 | 58.30 | 58.52 |
| 20 | 17 | 7 | 1.75 | 75 | 75 | 0 | 0 | 0 | 0 | 58.30 | 58.52 |
| 9 | 18 | 1.95 | 1.75 | 75 | 75 | $-\alpha$ | 0 | 0 | 0 | 18.27 | 16.83 |
| 7 | 19 | 4 | 2.5 | 90 | 100 | -1 | 1 | 1 | 1 | 65.15 | 68.95 |
| 19 | 20 | 7 | 1.75 | 75 | 75 | 0 | 0 | 0 | 0 | 58.30 | 58.52 |
| 13 | 21 | 7 | 1.75 | 49.8 | 75 | 0 | 0 | $-\alpha$ | 0 | 49.43 | 57.97 |

*$\alpha = 1.682$

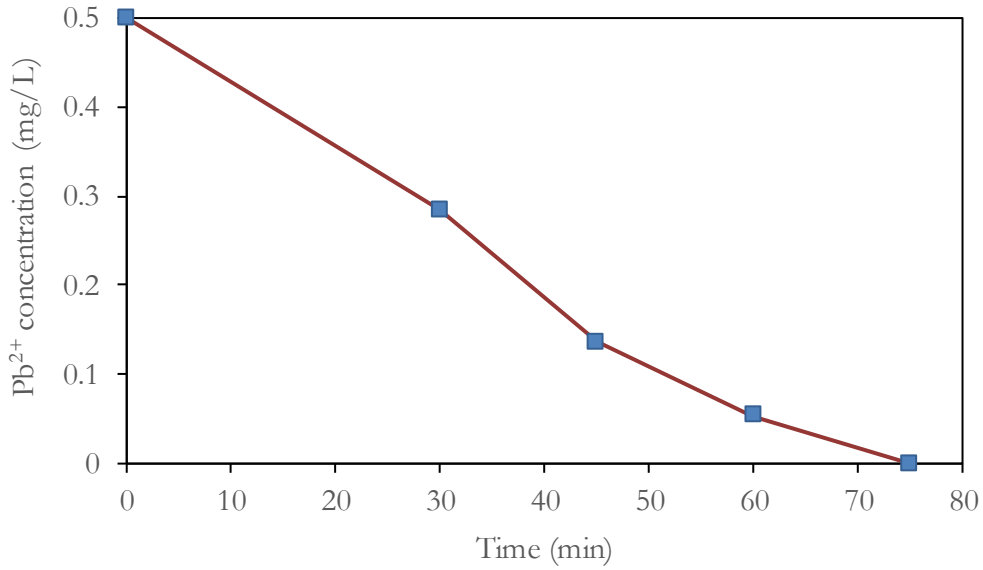


Figure 2. Variation of $Pb^{2+}$ concentration against time

Table 4. Model summary statistics

| Source | Std. Dev. | R-Squared | Adjusted R-Squared | Predicted R-Squared | PRESS | |
|---|---|---|---|---|---|---|
| Linear | 17.16 | 0.4959 | 0.3699 | 0.0796 | 8606.78 | Suggested |
| 2FI | 19.15 | 0.6080 | 0.2159 | -1.5843 | 24166.49 | |
| Quadratic | 5.87 | 0.9779 | 0.9263 | -0.2465 | 11656.75 | Suggested |
| Cubic | 0.0000 | 1.0000 | 1.0000 | | * | Aliased |

2FI is a 2-factor interaction model.

**ANOVA results**

From Table 5, the F value of the suggested model is obtained as 47.93, indicating that the model is significant. The signal-to-noise ratio was quantified regarding adequacy precision, including the expected values at different design points. A minimum value of adequacy precision ratio was reported to be four by Isar *et al.* (2006), whereas a much higher value of about 25.9 was achieved in this study. Therefore, the developed model is suitable for governing the design space.

The coded and actual models are presented in Equations (5) and (6), respectively, based on the significant terms.

$$Pb^{2+}\ \text{removal}\ (\%) = 58.52+1.34*X_1+8.20*X_2+8.29*X_3+24.26*X_4+17.16*X_1X_2 -13.94*X_1^2-2.60*X_2^2+4.74*X_3^2 \quad (6)$$

$$Pb^{2+}\ \text{removal}\ (\%) = 43.75+8.79*(\text{pH})-26.25*(\text{Adsorbent Dosage})-2.60*\text{Time} + 0.97*\text{Temperature}+7.63*(\text{pH}*\text{Adsorbent Dosage})-1.55*(\text{pH})^2 -4.63*(\text{Adsorbent Dosage})^2+0.02*(\text{Time})^2 \quad (7)$$

Table 5. ANOVA of $Pb^{2+}$ removal from wastewater

| Source | Sum of Squares | df | Mean Square | F Value | p-value Prob > F | |
|---|---|---|---|---|---|---|
| Model | 9067.5 | 8 | 1133.437 | 47.93322 | < 0.0001 | significant |
| $X_1$ | 24.56126 | 1 | 24.56126 | 1.038699 | 0.328232 | insignificant |
| $X_2$ | 918.0926 | 1 | 918.0926 | 38.82626 | < 0.0001 | significant |
| $X_3$ | 938.0655 | 1 | 938.0655 | 39.67091 | < 0.0001 | significant |
| $X_4$ | 3329.023 | 1 | 3329.023 | 140.7848 | < 0.0001 | significant |
| $X_1X_2$ | 975.7738 | 1 | 975.7738 | 41.2656 | < 0.0001 | significant |
| $X_1^2$ | 2917.811 | 1 | 2917.811 | 123.3946 | < 0.0001 | significant |
| $X_2^2$ | 101.7928 | 1 | 101.7928 | 4.304829 | 0.060174 | significant |
| $X_3^2$ | 336.4933 | 1 | 336.4933 | 14.23035 | 0.002661 | significant |
| Residual | 283.7541 | 12 | 23.64618 | | | |
| Lack of Fit | 283.7541 | 8 | 35.46927 | | | |
| Pure Error | 0 | 4 | 0 | | | |
| Cor Total | 9351.254 | 20 | | | | |

$R^2$ = *0.98, C.V. = 11.55 %, Adj* $R^2$ = *0.93, Pred* $R^2$ = *-0.25, Adeq precision = 16.48*

The temperature was found to be the most dominant factor in determining or predicting the $Pb^{2+}$ removal. This can be better appreciated from the Pareto chart as presented in Figure 3. The contribution of the temperature was about 34.89 %. Time followed with a distant second of about 9.83 %, while the least contributed factor was pH with about 0.26 %. Based on the factors' interactions, the square of pH contributed the most (30.58 %), followed by the product of pH and adsorbent dosage (10.23 %), with the least being the square of adsorbent dosage (1.07 %).

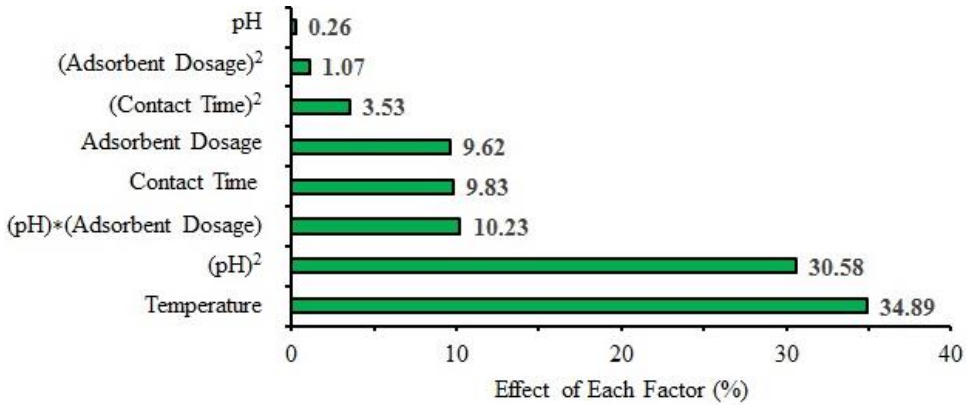


Figure 3. Pareto graph for $Pb^{2+}$ removal

## Discussions

### Validation of model

Figure 4 presents the plot of normal probability against studentized residuals. It can be seen that the residuals followed a normal distribution (i.e., no "S-shaped" pattern well away from the normal line) which is an indication that actual data transformations may not be required. Figures 5 and 6 present the studentized residuals against the predicted responses and run numbers, respectively. They provide a visual check for the assumption of constant variance. Since the plots show random scatter points, having no smiles or frowns pattern, there was no need for data transformation. This plot is also used

to examine outliers outside the red lines. Only one outlier resulted, as shown in Figure 6, indicating that the data generally fit the model. Therefore, there was no requirement for actual data transformations. The predicted responses against actual responses were plotted in Figure 7. This plot helps to detect a value or group of values that the model does not easily predict. The data points are split evenly by the 45° line, buttressing the earlier finding that there was no need for a transformation to improve the fit.

**Model graphs**

In terms of the three-dimensional plots, the effects of the experimental factors are presented in two forms: 3-D surface plots in Figures 8 – 10 and contour plots in Figures 11 – 13. Figures 8 and 11 show the interacting effect of pH and temperature on $Pb^{2+}$ removal at 75 minutes and adsorbent dosage of 1.75 g. The percentage removal of $Pb^{2+}$ was shown to be increasing with an increase in temperature. This behavior can be due to the fact that at high temperatures, the thickness of the boundary layer surrounding the catalyst particles decreases, resulting in an increased tendency of the metal ion to be adsorbed unto the surface of the adsorbent. However, concerning the increase in pH, there was an initial increase in the percentage removal of Pb2+ up to 7 before it decreased at a higher pH. This can be as a result of the high concentration of $H^+$ at lower pH values which tends to compete with the $Pb^{2+}$ for the adsorbent surface.

Similarly, the $Na^+$ from NaOH used in adjusting the pH could compete with the $Pb^{2+}$ at higher pH values. Figures 9 and 12 show the effect of the contact time and temperature on $Pb^{2+}$ removal. As the system was endothermic, high temperature favored the adsorption process, and hence percentage removal of the $Pb^{2+}$ increased. Similarly, an increase in the removal capacity of the $Pb^{2+}$ was observed with increasing time. This can result from the availability of sufficient time for the adsorption to take place before the saturation of the catalyst pore spaces. Lastly, Figures 10 and 13 present the combined effect of adsorbent dose and temperature. A progressive increase in adsorption efficiency was observed as the adsorbent dose was increased. This can be ascribed to the rise in available adsorption sites with an increase in the adsorbent dosage.

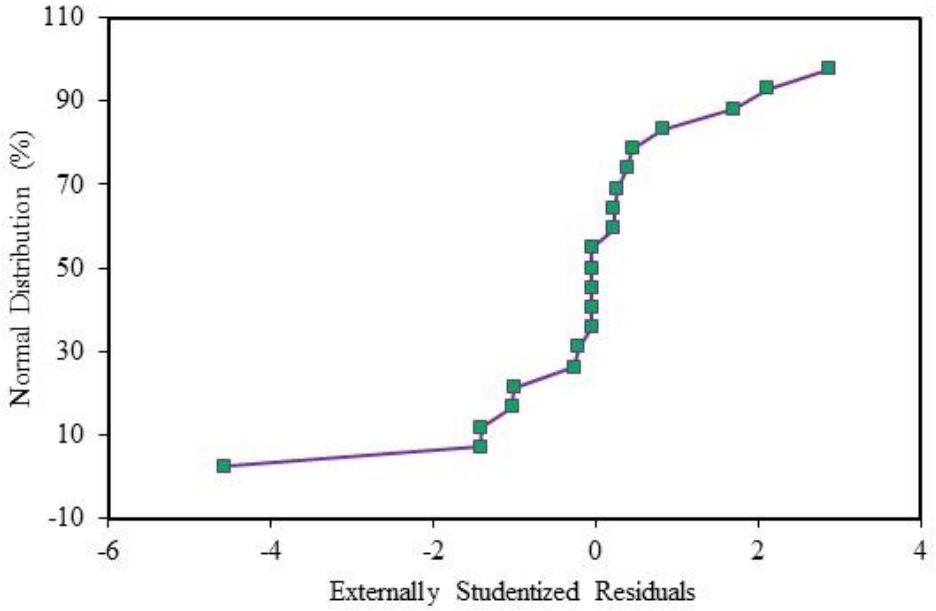


Figure 4. The normal probability vs. studentized residual plot for $Pb^{2+}$ removal

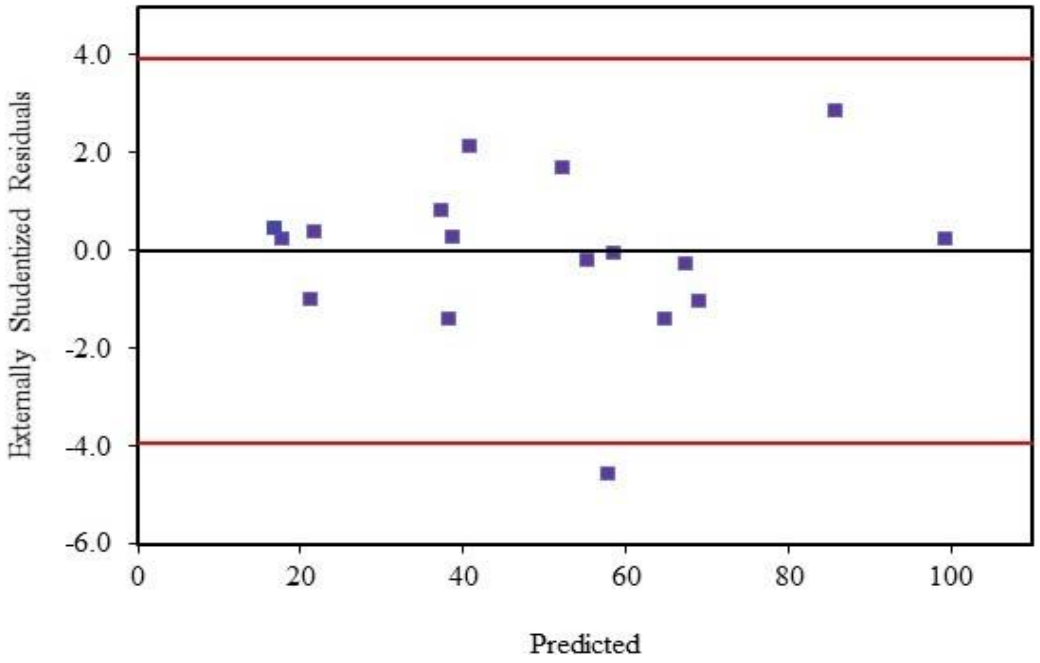


Figure 5. Internally studentized residual versus predicted $Pb^{2+}$ removal

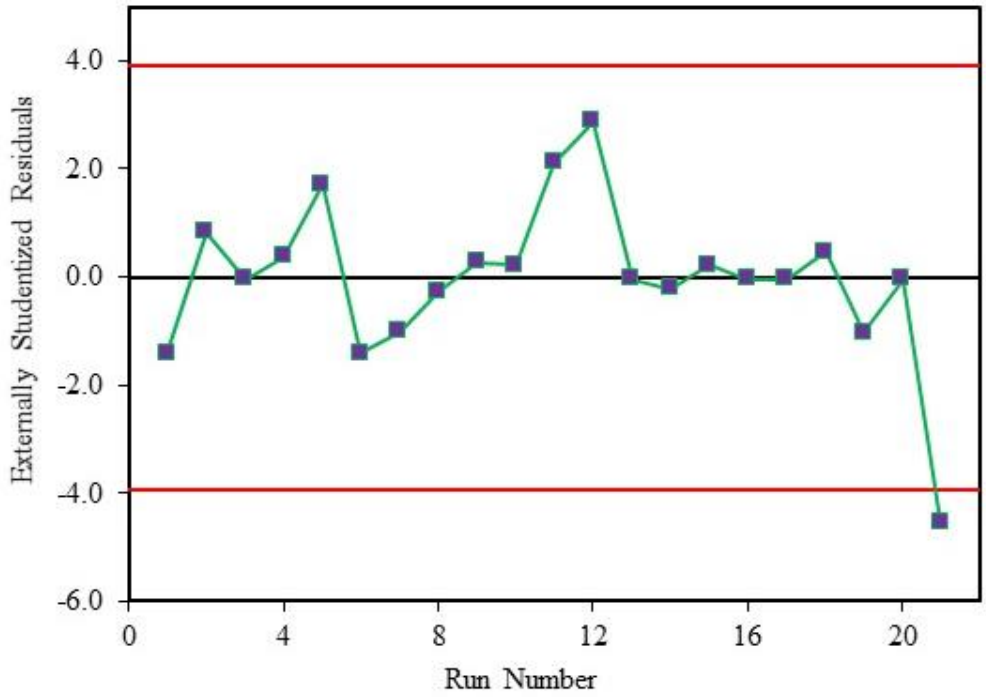


Figure 6. Internally studentized residuals versus the Run number

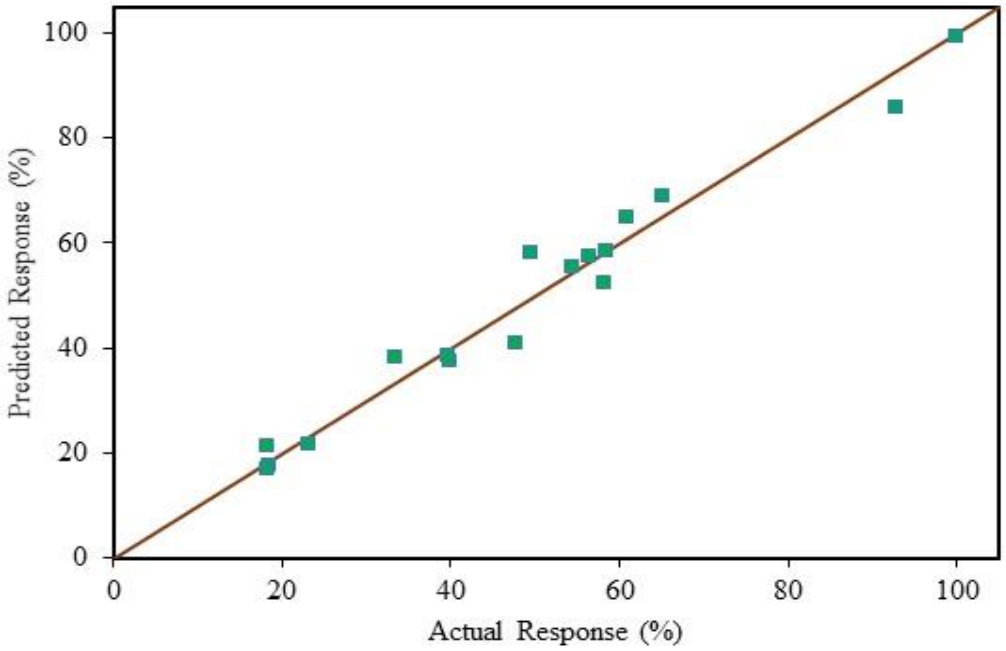


Figure 7. Predicted vs. actual responses

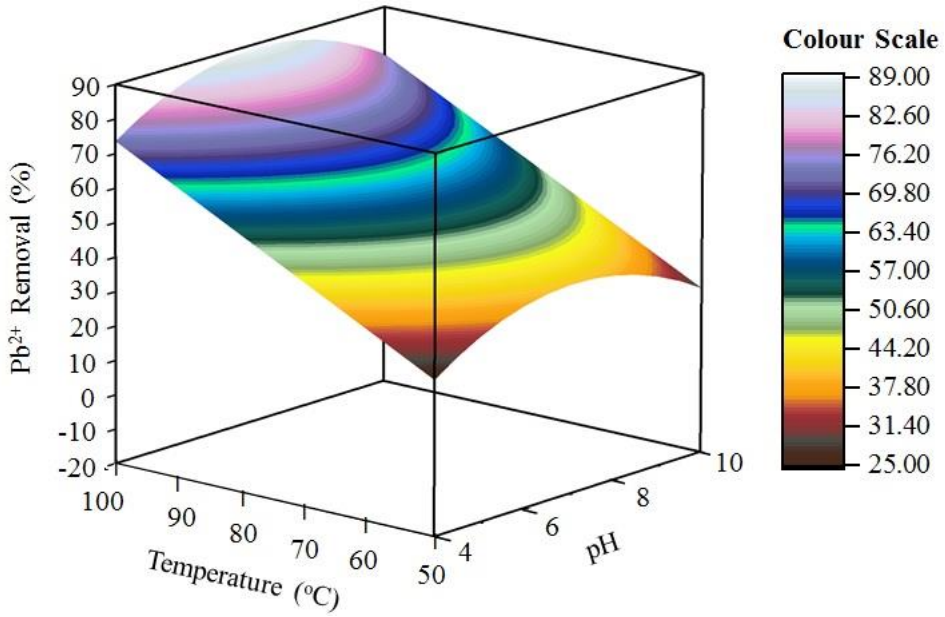


Figure 8. 3-D surface plot for interacting effects of temperature and pH on $Pb^{2+}$ removal at an adsorbent dose of 1.75 g and time of 75 min.

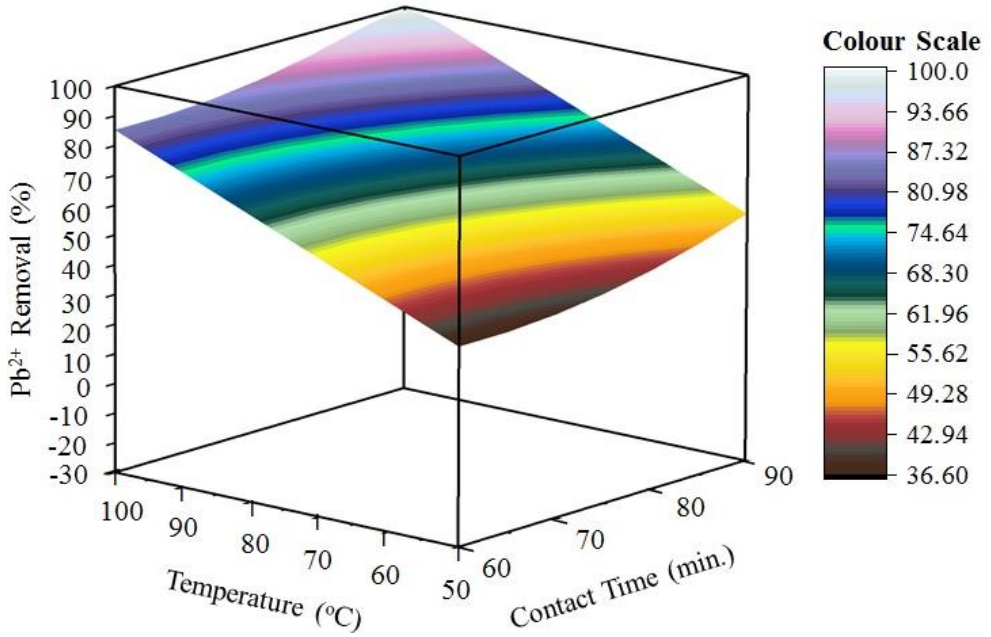


Figure 9. 3-D surface plot for interacting effects of temperature and time on $Pb^{2+}$ removal at an adsorbent dose of 1.75 g and pH of 7

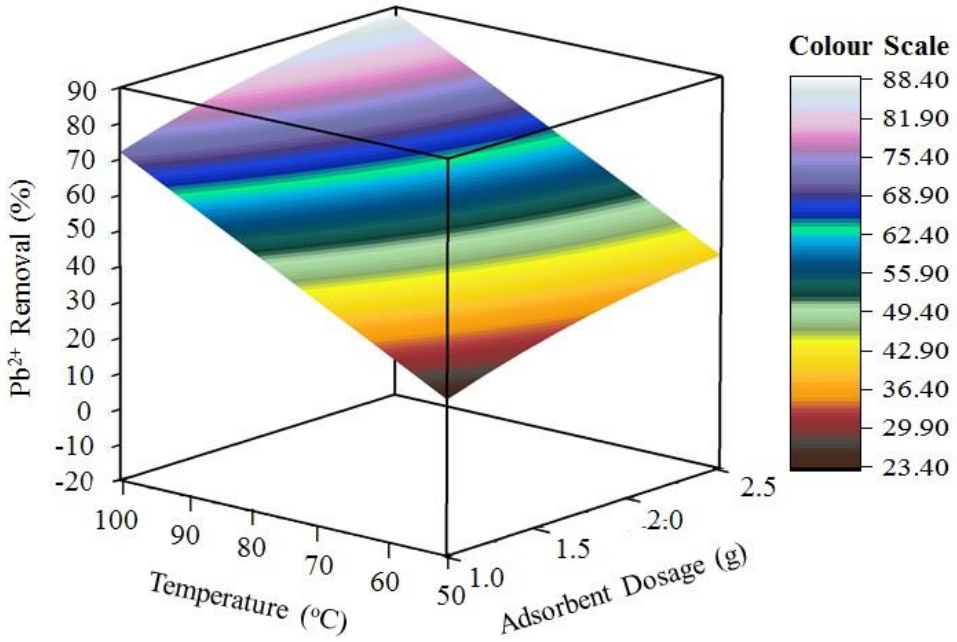


Figure 10. 3-D surface plot for interacting effects of temperature and adsorbent dose on $Pb^{2+}$ removal at a contact time of 75 min. and pH of 7

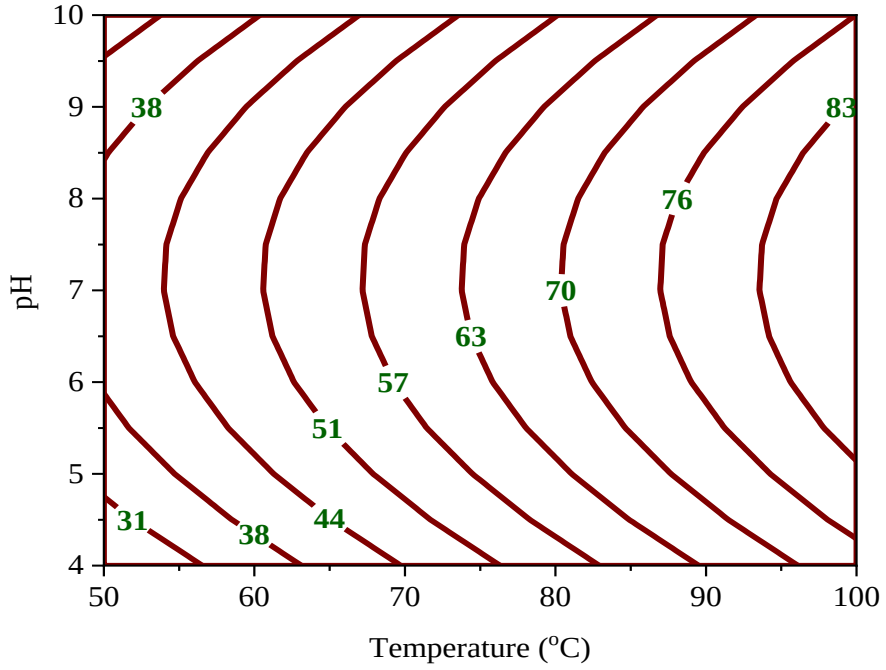


Figure 11. Contour plot for interacting effects of temperature and pH on $Pb^{2+}$ removal at an adsorbent dose of 1.75 g and time of 75 min.

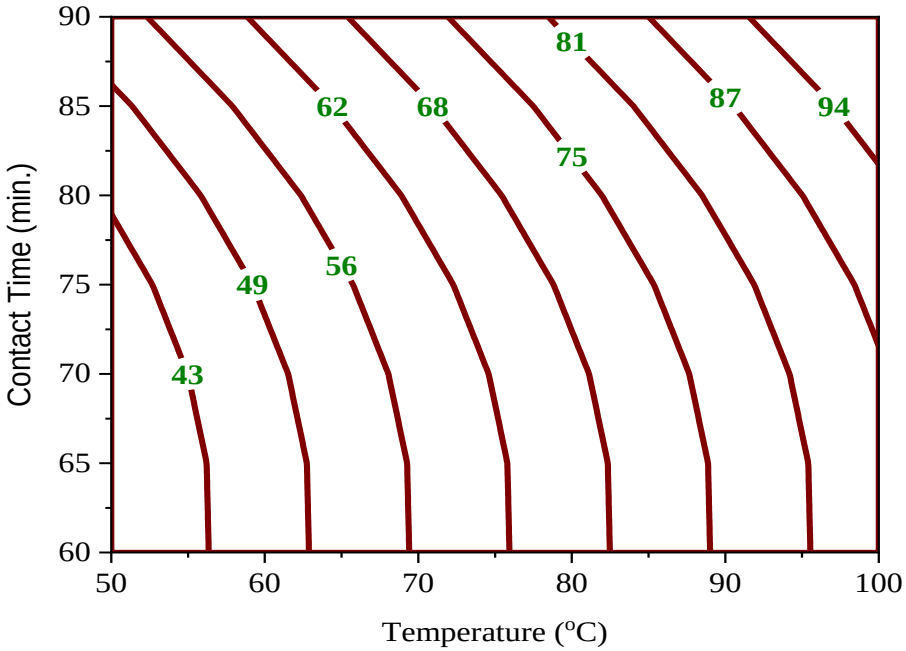


Figure 12. Contour plot for interacting effects of temperature and time on $Pb^{2+}$ removal at an adsorbent dose of 1.75 g and pH of 7

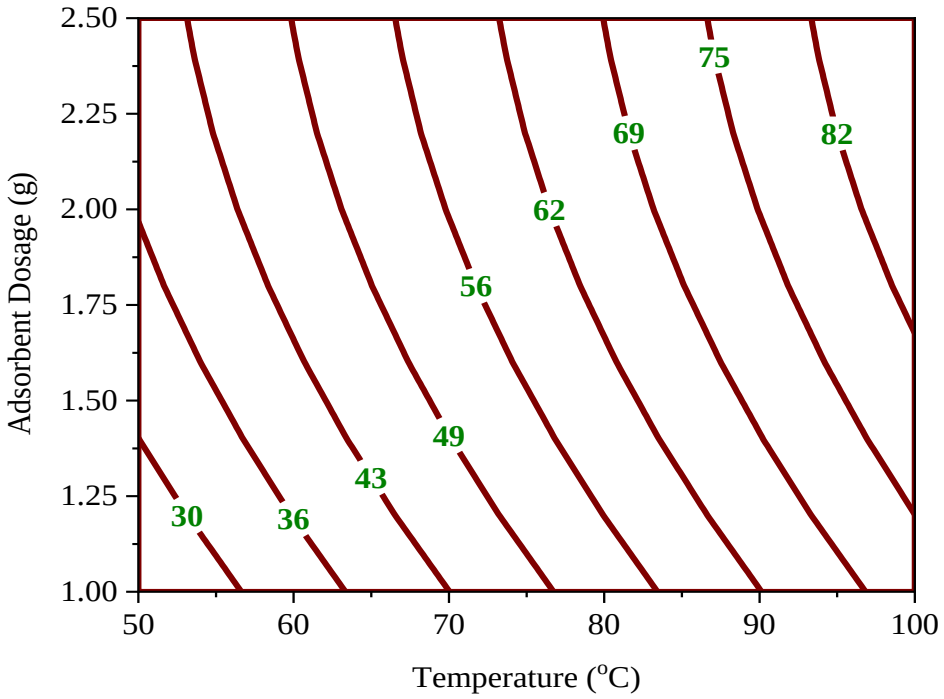


Figure 13. Contour plot for interacting effects of temperature and adsorbent dose on $Pb^{2+}$ removal at a contact time of 75 min. and pH of 7

## Conclusions

In this study, four variables central composite design under the response surface method (RSM) has been employed to investigate the effects of pH, adsorbent dose, contact time, and temperature on $Pb^{2+}$ adsorption onto spent FCC catalyst. The following conclusions could be drawn from the results. A second-order quadratic model equation was developed for predicting the response (percentage removal of $Pb^{2+}$) on overall experimental regions. From the sum of square values, the temperature was the most significant factor among investigated process variables. For maximum Pb2+ removal using reactivated spent FCC catalyst, the optimum condition was pH of 7, adsorbent dose of 1.75 g, contact time of 75 mins, and temperature of 117 °C.

## Acknowledgment

The authors gratefully acknowledge the Department of Chemical Engineering of Ahmadu Bello University, Zaria, for providing enabling environment for carrying out the research work.

## References

Afridi, H.I., Kazi, T.G. Kazi, G.H. Jamali, M.K. and Shar, G.Q. 2006. Essential trace and toxic element distribution in the scalp hair of Pakistani myocardial infarction patients and controls. Biological Trace Element Research, 113(1): 19-34.

Ahmad, F., Fouad, E. and Ahmad, N. 2014. Removal of lead from wastewater by adsorption Using Saudi Arabian Clay. International Journal of Chemical and Environmental Engineering, 5(2): 65-68.

Akçay, H. and Anagün, A.S. 2013. Multi response optimization application on a manufacturing factory. Mathematical and Computational Applications, 18(30): 531-538.

Ali, Z.T.A. 2019. Removal of lead ions from wastewater using crushed concrete demolition waste. Journal of Engineering Science, 26(4): 22-29.

Ani, J.U., Okoro, U.C. Aneke, L.E. Onukwuli, O.D. Obi, I.O. Akpomie, K.G. and Ofomatah, A.C. 2019. Application of response surface methodology for optimization of dissolved solids adsorption by activated coal. Applied Water Science, 9: 1-11.

Anupam, K., Dutta, S. Bhattacharjee, C. and Datta, S. 2011. Adsorptive removal of chromium (VI) from aqueous solution over powdered activated carbon: Optimisation through response surface methodology. Chemical Engineering Journal, 173: 135–143.

Begum, S., Yuhana, N.Y. Saleh, N.M. Kamarudin, N.N. and Sulong, A.B. 2021. Review of chitosan composite as a heavy metal adsorbent: Material preparation and properties. Carbohydrate Polymers, 259(1): 117613.

Behbahani, E.S., Dashtian, K. and Ghaedi, M. 2021. Fe3O4-FeMoS4: Promise magnetite LDH-based adsorbent for simultaneous removal of Pb (II), Cd (II), and Cu (II) heavy metal ions. Journal of Hazardous Materials, 410(1), 124560.

Bhattacharya, P., Banerjee, P. Mallick, K. Ghosh, S. Majumdar, S. Mukhopadhyay, A. and Bandyopadhyay, S. 2013. Potential of biosorbent developed from fruit peel of Trewia nudiflora for removal of hexavalent chromium from synthetic and industrial effluent: analyzing phytotoxicity in germinating Vigna seeds. Journal of Environmental Science and Health - Part A Toxic/Hazardous Substances and Environmental Engineering, 48(7): 706-719.

Bhaumik, M., Agarwal, S. Gupta, V. and Maity, A. 2016. Enhanced removal of Cr(VI) from aqueous solutions using polypyrrole wrapped oxidised MWCNTs nanocomposites adsorbent. Journal of Colloid and Interface Science, 470: 1-284.

Bingre, R., Louis, B. and Nguyen, P. 2018. An overview on zeolite shaping technology and solutions to overcome diffusion limitations. Catalyst, 8(4): 1-18.

Castro, L., Blázquez, M.L. González, F. and Muñoz, J.A. 2018. Heavy metal adsorption using biogenic iron compounds. Hydrometallurgy, 179: 44–51.

Cerqueira, H.S., Caeiro, G. Costa, L. and Ramoa-Ribeiro, F. 2008. Deactivation of FCC catalyst. Journal of Molecular Catalysis A: Chemical, 292: 1-13.

Chen, H.L., Tseng, Y.S. and Hsu, K.C. 2004. Spent FCC catalyst as a pozzolanic material for high-performance mortars. Cement and Concrete Composites, 26(6), 657-664.

Claros, M., Kuta, J. El-Dahshan, O. Michalička, J. Jimenez, Y.P. and Vallejos, S. 2021. Hydrothermally synthesized $MnO_2$ nanowires and their application in Lead (II) and Copper (II) batch adsorption. Journal of Molecular Liquids, 325, 115203.

Dakhil I.H. 2015. Adsorption of Lead from Industrial Effluents using Rice Husk. International Journal of Engineering and Management Research. 5(1): 109-116.

Daoud, W., Ebadi, T. and Fahimifar, A. 2015. Optimization of hexavalent chromium removal from aqueous solution using acid-modified granular activated carbon as adsorbent through response surface methodology. Korean Journal of Chemical Engineering, 32(6): 1119-1128.

Dhaouadi, F., Sellaoui, L. Hernández-Hernández, L.E. Bonilla-Petriciolet, A. Mendoza-Castillo, D.I. Reynel-Ávila, H.E. and Lamine, A.B. 2021. Preparation of an avocado seed hydrochar and its application as heavy metal adsorbent: Properties and advanced statistical physics modeling. Chemical Engineering Journal, 419(1), 129472.

El-Naggar I.M., Ahmed S.A. Shehata N. Sheneshen E.S. Fathy M. and Shehata A. 2018. A novel approach for the removal of lead (II) ion from wastewater using Kaolinite/Smectite natural composite adsorbent. Journal of Applied Water Science, 1(1): 1-13.

Erdem M., Ucar S. Karagöz S. and Tay T. 2013. Removal of Lead (II) Ions from Aqueous Solutions onto Activated Carbon Derived from Waste Biomass. Scientific World Journal, 2013: 1-7.

Fu, F. and Wang, Q. 2013. Removal of heavy metal ions from wastewaters: A review. Journal of Environmental Management, 92: 407–418.

Gao, L., Li, Z. Yi, W. Li, Y. Zhang, P. Zhang, A. and Wang, L. 2021a. Impacts of pyrolysis temperature on lead adsorption by cotton stalk-derived biochar and related mechanisms. Journal of Environmental Chemical Engineering, 9(4): 105602

Gao, C., Wang, X.L. An, Q.D. Xiao, Z.Y. and Zhai, S.R. 2021b. Synergistic preparation of modified alginate aerogel with melamine/chitosan for efficiently selective adsorption of lead ions. Carbohydrate Polymers, 256, 117564.

Griesiute, D., Gaidukevic, J. Zarkov, A. and Kareiva, A. 2021. Synthesis of β-Ca2P2O7 as an adsorbent for the removal of heavy metals from water. Sustainability, 13(14), 7859.

Isar J., Agawal, L. sarana, S. and Saxena, R.K. 2006. A statistical method for enhancing the production succinic acid from Escherichia Coli under anaerobic conditions. Bioresourse Technology, 97(13): 1443-1448

Kam, S.K., Hyun, S.S. and Lee, M.G. 2011. Adsorption of lead ion by zeolites synthesized from Jeju Scoria. Journal of Environmental Science International, 20(11): 1437–1445.

Kang, S.Y., Lee, J.U. Moon, S.H. and Kim, K.W. 2004. Competitive adsorption characteristics of $Co^{2+}$, $Ni^{2+}$, and $Cr^{3+}$ by IRN-77 cation exchange resin in synthesized wastewater. Chemosphere, 56: 141–147.

Kaoah, F., Boumaza, S. Berrama, T. Brahmi, L., Bendjama, Z. 2015. Response surface modeling and optimization of chromium (VI) removal from aqueous solution using date stones activated carbon in batch process. In: Progress in Clean Energy, 1: 671-682.

Kazi, T.G., Jalbani, N. Kazi, N. Jamali, M.K. Arain, M.B. Afridi, H.I. Kandhro, A. and Pirzado, Z. 2008. Evaluation of toxic metals in blood and urine samples of chronic renal failure patients, before and after dialysis. Renal Failure, 30(7): 737-745.

Kim, S.H., Chung, H. Jeong, S. and Nam, K. 2021. Identification of pH-dependent removal mechanisms of lead and arsenic by basic oxygen furnace slag: Relative contribution of precipitation and adsorption. Journal of Cleaner Production, 279, 123451.

Kuganathan, N., Anurakavan, S. Abiman, P. Iyngaran, P. Gkanas, E.I. and Chroneos, A. 2021. Adsorption of lead on the surfaces of pristine and B, Si and N-doped graphene. Physica B: Condensed Matter, 600, 412639.

Kuppusamy, S., Thavamani, P. Megharaj, M. Venkateswarlu, K. Lee Y.B. and Naidu, R. 2016. Oak (Quercus robur) acorn peel as a low-cost adsorbent for hexavalent chromium removal from aquatic ecosystems and industrial effluentsWater, Air, & Soil Pollution, 227(62): 1-11.

Le, T., Wang, Q. Ravindra, A.V. Li, X. and Ju, S. 2019. Microwave intensified synthesis of zeolite-Y from spent FCC catalyst after acid activation. Journal of Alloys and Compounds, 776, 437-446.

Manzoor, Q., Nadeem, R. Iqbal, M. Saeed, R. and Ansari, T.M. 2013. Organic acids pretreatment effect on Rosabourbonia phyto-biomass for removal of Pb(II) and Cu(II) from aqueous media. Bioresource Technology, 132: 446–452.

Mengistie, A.A., Siva, R.T. Prasada, A.V. and Singanan, M. 2008. Removal of lead(ii) ions from aqueous solutions using activated carbon from militia ferruginea plant leaves. Bulletin of the Chemical Society of Ethiopia., 22(3): 349-360.

Milošević, D., Lević, S. Lazarević, S. Veličković, Z. Marinković, A. Petrović, R. and Petrović, P. 2021. Hybrid material based on subgleba of mosaic puffball mushroom (Handkea utriformis) as an adsorbent for heavy metal removal from aqueous solutions. Journal of Environmental Management, 297, 113358.

Nair, V., Panigrahy, A. and Vinu, R. 2014. Development of novel chitosan–lignin composites for adsorption of dyes and metal ions from wastewater. Journal of Chemical Engineering, 254: 491-502.

Nakkeeran, E., Saranya, N. Giri-Nandagopal, M.S. Santhiagu, A. and Selvaraju, N. 2016. Hexavalent chromium removal from aqueous solutions by a novel powder prepared from Colocasia esculenta leaves. International Journal of Phytoremediation, 18 (8): 812-821.

Ogunleye, O.O., Ajala, M.A. and Agarry, S.E. 2014. Evaluation of biosorptive capacity of banana (Musa paradisiaca) stalk for lead (II) removal from aqueous solution. Journal of Environmental Protection, 5: 1451-1465.

Olayebi, O.O. and Adebayo, A.T. 2017. Removal of heavy metals from petroleum refinery effluent using coconut shell-based activated carbon. CARD International Journal of Engineering and Emerging Scientific Discovery, 2(20): 102 -117.

Pelalak, R., Heidari, Z. Khatami, S.M. Kurniawan, T.A. Marjani, A. and Shirazian, S. 2021. Oak wood ash/GO/Fe3O4 adsorption efficiencies for cadmium and lead removal from aqueous solution: Kinetics, equilibrium and thermodynamic evaluation. Arabian Journal of Chemistry, 14(3): 102991.

Qasem, N.A., Mohammed, R.H. and Lawal, D.U. 2021. Removal of heavy metal ions from wastewater: a comprehensive and critical review. NPJ Clean Water, 4(1): 1-15.

Qiu, B., Tao, X. Wang, H. Li, W. Ding, X. and Chu, H. 2021. Biochar as a low-cost adsorbent for aqueous heavy metal removal: a review. Journal of Analytical and Applied Pyrolysis, 105081.

Ramos-Guivar, J.A., Lopez, E.O. Greneche, J.M. Litterst, F.J. and Passamani, E.C. 2021. Effect of EDTA organic coating on the spin canting behavior of maghemite nanoparticles for lead (II) adsorption. Applied Surface Science, 538, 148021.

Rangabhashiyam S., Suganya E. and Selvaraju N. 2016. Packed bed column investigation on hexavalent chromium adsorption using activated carbon prepared from Swietenia Mahogani fruit shells. Journal of Desalination & Water treatement, 57(28): 13048-13055.

Ruiz, I., Corona-García, C. Santiago, A.A. Abatal, M. Arias, M.G.T. Alfonso, I. and Vargas, J. 2021. Synthesis, characterization, and assessment of novel sulfonated polynorbornene dicarboximides as adsorbents for the removal of heavy metals from water. Environmental Science and Pollution Research, 1-18.

Sada, S. 2018. Use of response surface optimization technique in evaluating the tool wear in a turning machine cutting process. Journal of Applied Science and Environmental Management, 22 (4): 483 – 487.

Samadi, A., Xie, M. Li, J. Shon, H. Zheng, C. and Zhao, S. 2021. Polyaniline-based adsorbents for aqueous pollutants removal: A review. Chemical Engineering Journal, 129425.

Saranya, N., Nakeeran, E. Giri-Nandagopal, M.S. and Selvaraju, N. 2017. Optimization of adsorption process parameters by response surface methodology for hexavalent chromium removal from aqueous solutions using annona reticulata linn peel microparticles. Water Science and Technology, 75: 2094–2107.

Shen, M., Song, B. Zeng, G. Zhang, Y. Teng, F. and Zhou, C. 2021. Surfactant changes lead adsorption behaviors and mechanisms on microplastics. Chemical Engineering Journal, 405: 126989

Waba, I.E., Abubakar, A. Yunusa, S. and Audu, N. 2020. Reactivation of spent FCC catalyst via oxidation and acid treatment. Applied Journal of Environmental Engineering Science, 6(1): 22–34.

Wang, X., Jing, S. Hou, Z. Liu, Y. Qiu, X. Liu, Y. and Tan, Y. 2018. Permeable, robust and magnetic hydrogel beads: Water droplet templating synthesis and utilization for heavy metal ions removal. Journal of Material Science, 53: 15009–15024.

Wang, S., Wu, J. Jiang, J. Masum, S. and Xie, H. 2021. Lead adsorption on loess under high ammonium environment. Environmental Science and Pollution Research, 28(4): 4488-4502

Xu, J. W. and Wang, Z. 2012. Adsorption of lead ion from waste water with hydrolytic lignin. Advanced Materials Research, 460: 368–371.

Yarkandi, N.H. 2014. Removal of lead (II) from waste water by adsorption. International Journal of Current Microbiology and Applied Sciences, 3(4): 207-228.

Yen, C.H., Lien, H.L. Chung, J.S. and Yeh, H.D. 2017. Adsorption of precious metals in water by dendrimer modified magnetic nanoparticles. Journal of Hazardous Materials, 322: 215–222.

Yu, L.J., Shukla, S.S. Dorris, L.K. Shukla, A. and Margrave, J.L. 2003. Adsorption of chromium from aqueous solution by maple saw dust. Journal of Hazardous Materials, 100: 53–63.

Yurtsever, M. and Sengil, I.A. 2008. Biosorption of PbII ions by modified quebracho tannin resin Journal of Hazardous Materials, 163(1): 58-64.

Zamora-Ledezma, C., Negrete-Bolagay, D. Figueroa, F. Zamora-Ledezma, E. Ni, M. Alexis, F. and Guerrero, V.H. 2021. Heavy metal water pollution: A fresh look about hazards, novel and conventional remediation methods. Environmental Technology & Innovation, 22, 101504.

Zhang, X., Yu, M. Li, Y. Cheng, F. Liu, Y. Gao, M. and Liang, Y. 2021a. Effectiveness of discarded cigarette butts derived carbonaceous adsorbent for heavy metals removal from water. Microchemical Journal, 106474.

Zhang, Y., Wang, Y. Zhang, H. Li, Y. Zhang, Z. and Zhang, W. 2021b. Recycling spent lithium-ion battery as adsorbents to remove aqueous heavy metals: adsorption kinetics, isotherms, and regeneration assessment. Resources, Conservation and Recycling, 156, 104688.

Zhao, H., Ouyang, X.K. and Yang, L.Y. 2021. Adsorption of lead ions from aqueous solutions by porous cellulose nanofiber–sodium alginate hydrogel beads. Journal of Molecular Liquids, 324, 115122.

Zhou, L., Xiong, W. and Liu, S. 2015. Preparation of a gold electrode modified with Au–$TiO_2$ nanoparticles as an electrochemical sensor for the detection of mercury(II) ions. Journal of Material Sciences, 50: 769–776.